# THE LAMBDA POINT EXPERIMENT IN MICROGRAVITY


J. A. Lipa, D. R. Swanson and J. A. Nissen,
I department of Physics, Stanford Universit y, Stanford, CA. 94305
and
T. C. P. Chui
Jet Propulsion Laboratory, California Institute of Technology, Pasadena, CA. 91109



in October 1992 a low temperature experiment was flown on the Space Shuttle in low earth orbit, using the JPL low temperature research facility. The objective of the mission was to measure the heat capacity and thermal relaxation of helium very close to the lambda point with the smearing effect of gravity removed. We describe the experiment with emphasis on the high resolution thermometry and the thermal control system. We also report preliminary results from the measurements made during the flight, and compare them with related measurements performed on the ground. The sample was a sphere 3.5 cm in diameter contained within a copper calorimeter of very high thermal conductivity. The calorimeter was attached to a pair of paramagnetic salt thermometers with noise levels in the $10^{-10}$K range. During the mission we found that the resolution of the thermometers was degraded somewhat, due to the impact of charged particles. This effect limited the useful resolution of the measurements to about two nanokelvins from the lambda point,



Submitted to Cryogenics (Space Cryogenics Workshop proceedings).

## INTRODUCTION

In the early 70's K. Wilson[1] developed a generalized treatment of cooperative transitions that for the first time made realistic predictions for the behavior of equilibrium thermodynamic properties in the transition region. His approach took into account fluctuation effects while avoiding a commitment to a precise Hamiltonian for the system, This new renormalization group (RG) formalism paved the way for numerical predictions of many 'universal' parameters - that is, system independent quantities - such as the exponents governing the divergence of various thermodynamic variables. These predictions were soon found to be in reasonable agreement with the general body of information on systems near a wide variety of cooperative transitions. However, the experiments were unable to give major attention to the deep asymptotic region, where the predictions were simplified and best established. Severe difficulties are encountered here, due to transition broadening associated with sample defects or with gravity, limiting the dynamic range of tests of the theory. For example, in solid systems impurity gradients and crystal imperfections invariably cause uncontrolled distortion of the singularity at a resolution t - $10^{-4}$ or $10^{-5}$ at best. Here t = I I-T/'I'$_c$I is a dimensionless temperature parameter, where $T_c$ is the transition temperature. Also, for t > $10^{-3}$ non-asymptotic corrections to the theory dictate either that additional parameters be carried in the curve fitting procedure used to extract the quantities of interest, or that the comparison with theory be terminated. In the case of the gas-liquid critical point, the fluid compressibility diverges at the transition, leading to substantial gravitational rounding for t ~ 1 $0^{-5}$. With dynamic ranges of 10 to 100, the resulting tests of the. theory are somewhat limited in their utility. To perform better tests it is necessary to look for unusual situations where these problems can be overcome.

We are very fortunate that there is one transition, the lambda transition of helium, that is very sharp, and where measurements are presently limited only by technology. This transition occurs at $T_\lambda$ = 2.1768 K, when the helium liquid is at its vapor pressure. Because of the strain-free nature of the fluid and its relatively low compressibility, values of t as small as $10^{-7}$ can be reached on earth before intrinsic distortion is encountered, with sample heights of the order of millimeters. The ultimate limit is usually encountered when finite size effects[2] become appreciable, generally near t ≈ 3x10-8. In space, the lambda transition may be sharp to t - 10-12 or S$0^3$, in optimal conditions. All other systems pale by comparison. At these resolutions, the challenge is more to develop a measurement technique than to obtain a suitable sample, Since 1975 we have been developing the technology to perform a high resolution heat capacity experiment near the lambda point on the Space Shuttle. Since the low frequency acceleration environment of the Shuttle is quite variable, the experiment was conservatively optimized for a level of 3x10-4 g, and a corresponding resolution of t ~ 4x1 $0^{-1}$0. This is about two orders of magnitude higher resolution than is possible on earth, allowing a substantially improved measurement of the heat capacity curve and estimate of the exponent $\alpha$ characterizing its divergence at the transition temperature. The data could lead to a much stronger confrontation between theory and experiment than has been possible to date, and hopefully will provide a stimulus for improved models of cooperative phenomena. Also, it will allow exponent estimates deep in the asymptotic region which are of comparable accuracy to previous results further from the transition. These estimates will be extremely useful in testing the validity of the asymptotic representation assumed in all theoretical models so far developed. In this paper we describe the technology that was developed to make the measurements, and discuss preliminary results from the mission, which was flown in October 1992.

## INSTRUMENT DESIGN

The most significant problems one is faced with when contemplating the design of a high resolution heat capacity experiment are temperature resolution and thermal control, Conventional thermometry, e.g. germanium resistance thermornetry, allows a resolution approaching $10^{-7}$ near $T_\lambda$ with low power dissipation, but higher resolution means higher power input which rapidly leads to unacceptable thermal gradients. Since the goal of our experiment was to achieve a resolution of $4x10^{-10}$, we were immediately faced with the development of a new high resolution thermometer (HRT). The new device makes use of superconducting technology to achieve a resolution of about $3x10^{-10}$K ina 1117, bandwidth with negligible power dissipation, and is described below.

To actually make the heat capacity measurements with the desired resolution it is necessary to meter energy into the sample in units as small as $10^{-9}$C Joules, where C is the heat capacity of the sample. In our case, for a heater that operates for a few seconds, this corresponds to powers of the order of $10^{-8}$W. In addition, during the period used to measure the corresponding temperature rise, the variability of the background power input must be less than ~ $10^{-10}$ W. This means that very careful thermal control of the sample environment is necessary. To achieve this, we built a four stage thermal control system which used a HRT on the inner stage as a fine control sensor, This control system was the major portion of the low temperature apparatus which comprised the flight instrument. It is also described below. A third item of great importance is a helium dewar capable of operating in space. We made use of the previously flown JPL low temperature facility which has the capability of easily operating near 2 K in zero gravity. The performance of this system is reported separately in these proceedings in a paper by D. Petrac, U. Israelsson and T. Luchik.

## THERMOMETRY

The construction of the HRT has been described in some detail elsewhere[4] Briefly, it consists of a superconducting tube surrounding a crystal of paramagnetic salt which is thermally coupled to the experiment. The tube applies a fixed magnetic field to the salt. As the temperature of the experiment changes, so does the magnetization of the salt, due to its Curie law susceptibility. A superconducting pickup loop is wound on the salt and couples the changes in magnetization to an rf SQUID magnetometer for readout. A schematic view of the device is shown in figure 1. The salt pill consists of a single crystal of copper ammonium bromide, $Cu(NH_4)_2Br_4.2H_2O$, grown from aqueous solution onto a grid of 76 fine copper wires which are used for thermal contact to the sample. This salt material has a magnetic transition near 1.8 K and a highly temperature dependent susceptibility near the lambda point. The pickup coil is formed from niobium-titanium wire with an open-winding geometry used to maximize the enclosed volume of salt while simultaneously matching the self-inductance to the SQUID input. The windings are held together with GE 7031 varnish and fit snugly on the cylindrical salt pill. The coil and salt pill are inserted into a sapphire holder, Sapphire was chosen for its high thermal conductivity, absence of Johnson noise currents and low thermal expansion coefficient. This latter property was used to obtain a shrink fit between the holder and the niobium flux tube, minimizing the relative motion between the coil and the tube, and thereby contributing to the high stability and low vibration sensitivity of the HRT. One end of the holder was metallized and soldered to a copper post thermally coupled to the experiment. The leads from the pick-up coil were tightly twisted together, passed through a Nb-Ti tube for shielding, and attached to a SQUID. A heat-switch consisting of a piece of 0.003 cm diameter manganin wire was wrapped tightly onto one lead near SQUID input terminals. By activating the heat-switch with a 10 mA current the HRT lead could be heated above its superconducting transition temperature, causing any current flowing in the pickup coil to rapidly decay. These currents must be carefully controlled as they affect the calibration of the thermometers by inducing an additional magnetic field on the salt.

For a field of 100 G trapped in the flux tube, the sensitivity of a HRT is typically in the range 3- $4\Phi_0/\mu K$, where $\Phi_0$ is the quantum of magnetic flux. Since the SQUID noise level is at least as low as $10^{-4}\Phi_0/\sqrt{Hz}$, a resolution of ~ $3\times10^{-11}$ deg is possible. In general, a much larger noise level is seen. The noise characteristics of a HRT can be studied by attaching it to a large thermal reservoir and reducing the heating rate to below $10^{-12}$ K/sec by careful thermal control. A typical noise spectrum obtained this way is shown in figure 2. With such a high temperature resolution, the possibility of noise contributions from various fluctuating quantities must be considered. The data in the figure can be compared with the predictions of the fluctuation-dissipation theorem developed by Callen and

Welton[5]. When this is done[6], the best fit is obtained with the temperature fluctuation model. This is shown by the solid line in the figure, with no adjustable parameters. For comparison, the SQUID noise contribution is also shown in figure 2. The HRT noise per unit bandwidth in the low frequency region is normally about $3 \times 10^{-10}$ K/√Hz. The absolute drift rate of the HRTs has been found to be $\sim 10^{-14}$ K/see by observing the apparent location of the lambda transition as a function of time in various high resolution experiments.

## THERMAL CONTROL SYSTEM

The thermal control system used in the flight experiment consisted of a multi-stage thermal platform located in the helium dewar, and an electronics assembly that houses the servos for the various levels of thermal control, along with the readout electronics for the HRTs. It has been described in some detail elsewhere[7]. The platform (shown in figure 3) consists of a vacuum shell about 20 cm in diameter and 60 cm long surrounding four thermal control stages in series and the calorimeter (stage 5). A set of four HRTs are housed in the lower part of the assembly and are surrounded by a thermal shield attached to the innermost stage of the control system. A solenoid is mounted on the outside of the lower portion of the vacuum can to allow the application of a magnetic field to the HRTs during initial cool-down. A cylindrical superconducting shield open at one end surrounds the assembly to minimize the effects of external fields on the HRTs.

A tripod structure with legs of stainless steel tubing hangs from the lid of the vacuum shell. Three OFHC copper rings intersect the legs of the tripod at intervals of about 3 cm. These rings form the first three stages of the isolation system and also serve to stiffen the tripod. The rings are tight fitting on the legs and are attached by brazing. While the legs were mechanically supported by the vacuum can top plate, they were thermally attached to a copper ring in the center of the cylindrical wall of the vacuum shell to provide better cooling by the helium bath. Each stage has a germanium resistance thermometer (GRT) and heater for temperature readout and servo control. The thermal isolation of these stages is sufficient to reduce the thermal inhomogeneities to the point where they are dominated by the dissipation in the GRT and the heater on stage 3. This effect is then limited by reducing the offset between the operating temperatures of stages 2 and 3 to the minimum possible value.

Stage 4 has a more complex structure, consisting of a ring, shield and HRT support assembly all formed from annealed OFHC copper, The HRT support assembly provided attachment points for two HRTs and clearance holes for the two stage 5 HRTs. The shield completely surrounds stage 5 and all four HRTs. It acts as a baffle for stray thermal radiation and a shunt for residual gas conduction. Stage 5 is located near the apex of the tripod at the ends of the legs. It consists of a high purity copper calorimeter and a pair of HRTs. The configuration was designed to minimize temperature offsets between the HRTs and the calorimeter body. This was done by providing large area contacts between the HRTs and the calorimeter, thermally separated from the tripod attach point. Stages 4 and 5 were also equipped with GRTs and heaters. Those on stage 4 were used for thermal control which had two modes: a coarse mode with the GRT as sensor, and a fine mode with the HRT as sensor. Gradients in this stage were again minimized by reducing the temperature offset to stage 3. On stage 5, thermal gradient control was improved by deactivating the GRT during high resolution measurements and using the heater only when step temperature changes were desired. All the HRTs were grouped together for convenient charging by the solenoid on the vacuum can.

In operation, temperature stability of stage 5 was obtained by fine adjustment of the set point of stage 4. The limiting factor on thermal control of the calorimeter appeared to be variations in stray power pickup in the circuits attached to stage 5. For these circuits special precautions were taken: all leads to the calorimeter were thermally anchored at all stages using sapphire stand-off posts to minimize capacitance to ground. Also, these leads were equipped with capacitance shunts where they entered the helium dewar, which formed a complete metallic enclosure around the thermal control system. For wiring to other stages, similar techniques were used, except that the sapphire was replaced with copper. The calorimeter was also thermally connected to stage 4 by four capillary gas lines and two HRT pickup loops with Nb-Ti shields. Special clamps were built to thermally anchor these lines to the isolation stages using iridium foil as a thermal contact material. All leads and lines were fabricated from low thermal conductivity materials. In the case of leads to heaters, niobium wire was used, both to allow accurate heat input measurements, and to avoid losses due to lead heating.

The calorimeter was a copper sphere of 3.5 cm internal diameter and 2 mm ???? wall thickness. The copper[8] was 99.9999% pure and highly annealed, with a measured residual resistance ratio of over 4000. It was formed by electrical discharge machining and electron beam welding. On the end opposite from the HRTs was a pressure-actuated valve used to seal the chamber after filling and allow evacuation of the fill line. The valve was formed by pressing a beryllium-copper knife edge against a gold-plated copper flat. It was found to be highly reliable during three years operation. The heaters and GRTs were attached to the spherical wall of the tank.

The leads from the HRTs were thermally anchored to each stage of the thermal control system and were attached to SQUID magnetometers. These were mounted on an independent, single stage thermal platform also supported from the vacuum can top plate. This arrangement was necessary to minimize the effect of the temperature coefficient of the SQUID on the HRT output. This platform was stabilized to < $10^{-4}$ K using standard GRT techniques. The SQUIDS were housed in individual niobium shields[9] with magnetic field attenuation factors of - $5x10^9$, and close fitting Cryoperm shields.

Also attached to the top plate was a charcoal adsorption pump assembly used to maintain a high vacuum inside the thermal control system. This pump was equipped with a heater and thermometer to allow regeneration as necessary. With no exchange gas used in the system the base pressure was well below 10-9 torr, the limit of our measuring technique, When helium exchange gas was introduced, the pump-down time constant was on the order of a day, dependent on the vacuum can wall temperature. For pressures significantly above $10^{-9}$ torr, the effect of gas conduction between stage 4 and the vacuum can is detectable and additional thermal gradients will be present in all extended assemblies. The gas will also generate an induced temperature gradient in stage 5 due to that in stage 4. With a pressure of 10-9 torr these gradients are estimated to be on the order of $10^{-10}$ K/cm in stage 5.

The thermal control system is also equipped with a device to allow rapid cooling which is attached to all stages. It consists of a loop of capillary tubing through which helium gas or superfluid can be circulated. This arrangement is very advantageous when multiple sweeps through wide temperature ranges are needed. It was used only in ground testing. All control elements on stages 4 and 5 were duplicated as previously described to decrease the impact of a hardware failure during the Shuttle mission.

## FLIGHT EXPERIMENT

The instrument was maintained at 4 K or colder for the entire 18 months before launch. In this period extensive tests were performed to verify its performance under various conditions, In addition a number of preflight calibrations and heat capacity measurements were completed. This data was very useful for deciding the details of the flight measurement sequence and for studying the general behavior of the system. Shortly before launch the helium in the dewar was converted to the superfluid state and the instrument cooled to about 1.7 K. The instrument vacuum space was filled with $^3He$ exchange gas at about 5 mm pressure to maintain a thermal short to the bath during launch. If this was not done, there was a high risk that the HRTs on the thermal control system would warm above their superconducting transition temperature, substantially reducing their sensitivity. About two hours into the flight the system was activated and the exchange gas pump-out procedure was started. This consisted of first venting to space until a pressure of 0.5 torr was reached, and then sealing off and using a charcoal cryopump together with a thermal cycle of the dewar. During the course of the mission the pressure in the instrument could be monitored by observing the power required to maintain stage 4 of the thermal control system near the lambda point. It was found that the flight pump-down rate was significantly less than on the ground. Figure 4 shows the results for the two situations. The reason for the slower rate is not yet known, but it is possibly due to more uniform cooling of the instrument walls in microgravity.

When the pressure approached the $10^{-8}$ ???? torr range the main measurement sequence was started. The first event of significance in the experiment was the generation of a small bubble in the calorimeter, used to establish a thermodynamic path close to constant pressure for the heat capacity measurements measurements. This event occurred as the calorimeter warmed through 2.079 K and was detected by observing the small sudden cooling generated by the first order phase transition. Before the system could be used for high resolution work, the various stages needed to be brought to their normal operating temperatures. These temperatures were kept as close as practical to that of the calorimeter. If all temperatures were held equal, thermal gradients would decrease rapidly as one moved to the inner stages. However, small temperature offsets are needed to provide some cooling power for servo control. During ground-based tests we found that offsets as small as 1 mK between neighboring stages were sufficient to give servo response times of a few tens of seconds. With thermal resistances between stages of about $10^4$ K/w, the corresponding control powers were in the range $10^{‘6}$ - $10^{-7}$w. A typical temperature profile of the thermal control system consists of stage 5 at a given operating temperature and stage 4 in equilibrium with it, and stages 3, 2 and 1 servoed at 1, 10 and 30 mK below stage 4, After the system was thermally aligned the calorimeter was warmed to the starting temperature for the HRT calibration sequence.

Up to this point stage 4 was operated in the coarse mode, but after the thermal transients had settled, and the fine mode was activated. The final step was to reduce the drift rate of the calorimeter temperature to an acceptable value. To do this the output of the primary stage 5 HRT is monitored and the drift rate $dT_5/dt$ calculated. From this quantity the change in the stage 4 set point required to drive it to null is estimated using the relationship:

$$T_4 - T_5 = (dT_5/dt) * C_5 / K \qquad (1)$$

where $K$ is the thermal conductance between stages 4 and 5, and $C_5$ is the calculated heat capacity of stage 5. After the set point is changed the process is iterated until the stage 5 drift rate falls below a predetermined level. This procedure was implemented by a straightforward computer algorithm. Three iterations were generally sufficient to reduce the drift rate by four orders of magnitude, approaching $10^{’12}$ K/s.

The calibration procedure consisted of a set of 1 rndeg heating steps separated by 45 seconds of equilibration. The data was analyzed on the ground and verified to be close to the preflight results. Figure 5 shows the results of the calibration and a comparison with earlier data obtained from ground measurements. The second phase of the calibration procedure was to measure the switched stray power in the heater circuit, This was done by measuring the heat capacity of the sample as a function of power dissipated in the heater at nominally constant temperature. Any power change that is unaccounted for causes the apparent heat capacity to be inversely proportional to the measured power. The results of this procedure are shown in figure 6. The stray power was estimated to be less than 10-10 W. After the calibration was completed, heat capacity measurements were commenced and continued for the rest of the flight. The quantity of energy dissipated in the heater was determined from a look-up table based on the distance from the lambda point. This distance was determined from each heat capacity measurement by comparing it with a model of the singularity. After the lambda point had been reached the first time, this method was dispensed with and the apparatus was operated manually by ground command.

A sequence of measurements near the start of the mission is shown in figure 7. Figure 8 shows the preliminary heat capacity values from this period on a semi-logarithmic scale. For comparison the broken line shows the expected values from a model based on ground results. Figures 9 and 10 show the preliminary results at higher resolution.

When measurements at the highest resolution were attempted, excess noise was found on the outputs of the HRTs. This was traced to the heat dissipation due to cosmic rays and other particles passing through the sensitive element of the HRTs. A comparison of the HRT output on the ground and in space is shown in figure 11. A slow variation in the drift rate of the calorimeter was also detected under nominally steady conditions. This was found to be due to charged particles dissipating energy in the copper calorimeter. To obtain accurate heat capacity results it is necessary to correct the raw data for the particle heating effects. Heating of the calorimeter by charged particles was anticipated so the experiment carried a charged particle monitor for use as an indicator of periods of severe heating. The variation of the charged particle counting rate over a 24 hr. period is shown in figure 12. The four channels of data correspond to different energy bands for the particles. The background level of from 2 to 5 counts per second corresponds to the cosmic ray flux and the higher peaks are due to the particles trapped in the radiation belts. Models are being developed to correct the high resolution results for the heating effects. It is expected that a resolution of about 2 nanodegrees will be possible with good accuracy. Additional heat capacity data can be extracted from the cooling curves obtained when the calorimeter temperature is reset below the lambda point, However it is apparent that for this case careful modeling of thermal relaxation effects close to the transition will be needed.

Above the transition the calorimeter temperature initially overshoots when a heat pulse is applied due to the finite thermal conductivity of the helium. From the resulting relaxation data an estimate of the thermal conductivity can be obtained. A typical response curve to a five second heat pulse is shown in figure 13. Also shown is simple exponential fit to the relaxation data. When fully analyzed we expect this data to give thermal conductivity data for helium in the normal phase to within about ten nanodegrees of the transition. Enough data was collected in this region to bridge to ground-based thermal conductivity data further from the transition.

## ACKNOWLEDGEMENTS

W e wish to thank the Microgravit y office of NASA for its support with contract #JPL-957448, and the members of the I .PE program at Stanford and JPL for their many contributions to the program, and Ball Aerospace for construction of major portions of the flight instrument.

## REFERENCES

1. K. G. Wilson, *Phys.* Rev. B 4,3174 (1971 ).
2. F. M. Gasparini and I. Rhee, *Progr.* Low *Temp. Phys.* **13, 1** (1992).
3. J. A. Lips, *75th Jubilee Conference on Helium-4*, ed. J. G. M. Armitage (World Scientific, Singapore, 1983), p. 208.
4. J. A. Lipa, B. C. Leslie and T. C. Wallstrom, Physics 107 B, 331 (1981); T. C. I? Chui and J. A. Lipa, Proc. 17th Internat. Conf. on Low Temp. Phys. (Karlsruhe, 1984), p.931; M. J. Adriaans, T. C. P. Chui, M. Ndesandjo, D. R. Swanson and J. A. Lipa, Physics B 169, 455 (1991); and T. C. P. Chui, D. Swanson, M. J. Adriaans, J. Nissen, and J. A. I tips, *Proc.* 7th *Int. Conf. on Tem* p., in press (April, 1992).
5. H. B. Callen and T. A. Welton, *Phys. Rev.* 83,34 (1951).
6. T. C. P. Chui, D. Swanson, M. J. Adriaans, J. Nissen, and J. A. Lipa, *Phys.* Rev. *Lett.* 69, 3005 (1992).
7. J. A. Lipa, T. *C. 1?* Chui, J. Nissen and D. Swanson, *Proc.* 7th *Int. Conf. on Tem* p., in press (April, 1992).
8. Nippon Mining Co., Japan, high purity copper, grade 6N, RRR approx. 4000.
9. K. W. Rigby, Rev. Sci. Instrum. 59,156 (1988).

## FIGURE CAPTIONS:

Figure 1: Schematic diagram of the high resolution thermometers.

Figure 2: The noise spectra of (a) a SQUID magnetometer, and (b) a high resolution thermometer. The solid line in (b) is the prediction of the fluctuation-dissipation theorem with no adjustable parameters.

Figure 3: Schematic view of the thermal control system and calorimeter.

Figure 4: Gas pressure in the instrument vacuum space vs. time.

Figure 5: Deviation plot of the HRT/GRT calibration data as a function of temperature. Triangles: flight data; crosses: ground results.

Figure 6: Dependence of apparent heat capacity on pulse power, measured well away from the lambda transition. Solid curves show the effect expected by $10^{-10}$ W stray power. Broken curves show the expected 10 band from the uncertainties in the measurements, based on ground information.

Figure 7: Stage 5 HRT output vs. time during low resolution heat capacity measurements as the lambda transition was approached.

Figure 8: Wide range heat capacity data obtained early in the mission. broken curve shows expected results based on earlier work.

Figure 9: Stage 5 HRT output vs time during high resolution heat capacity measurements. Each step corresponds to a temperature change of about 4 nanodegrees. Solid line is a fit to the data used to estimate the individual step heights.

Figure 10: Preliminary heat capacity data from a single high resolution pass up to the transition. The two symbols correspond to the two I IRTs on the calorimeter.

Figure 11: Comparison of HRT noise on the ground and in orbit. The spikes appear to be due to the impact of high-Z cosmic rays on the salt pill.

Figure 12: Charged particle count rate over a 24 hr. period. Four channels correspond to different energy ranges.

Figure 13: Data from a single heat pulse above the transition. Overshoot *is* due to the presence of normal helium in the calorimeter. Solid line is a simple exponential fitted to the high temperature data.

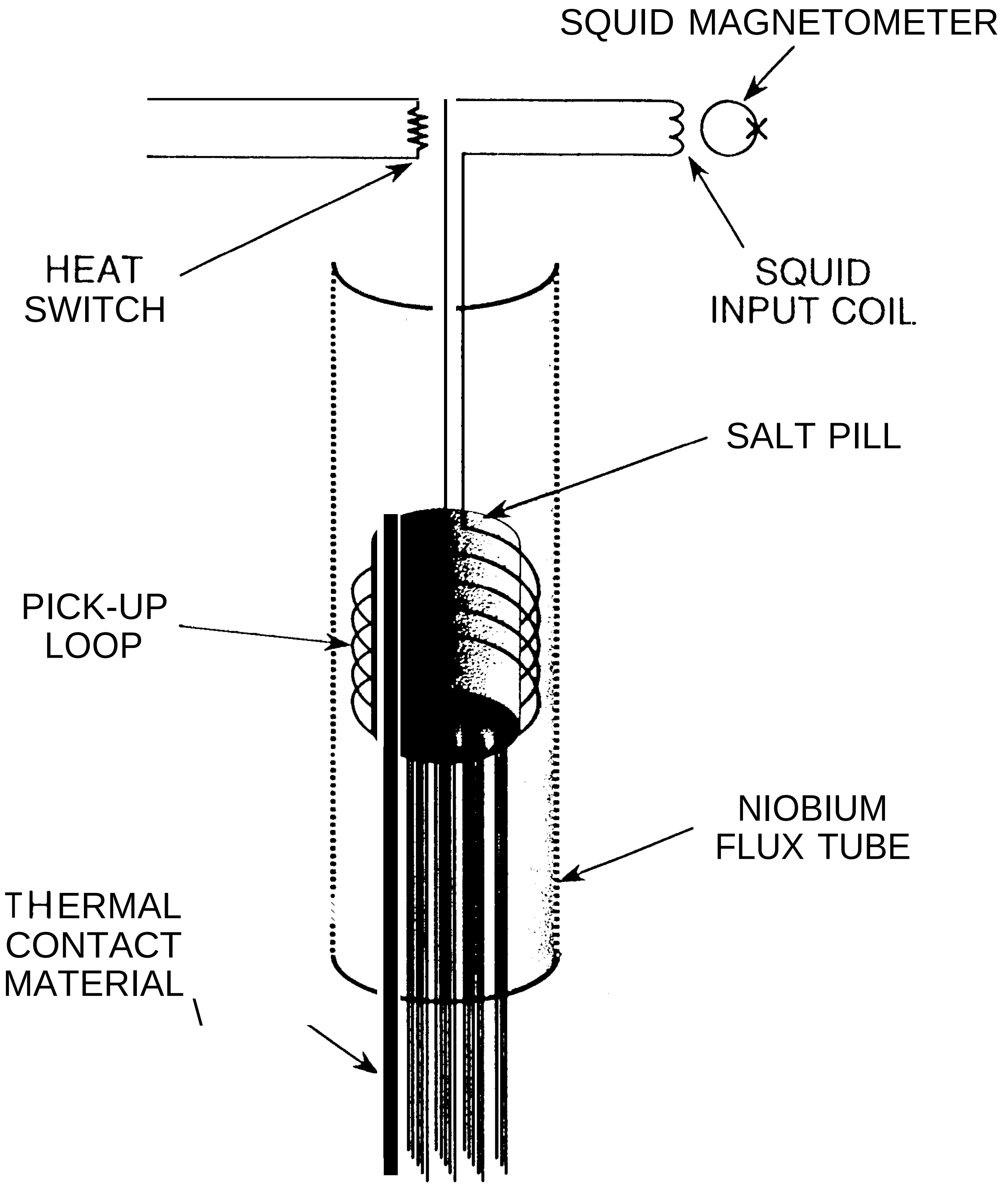
SQUID MAGNETOMETER
HEAT SWITCH
SQUID INPUT COIL
SALT PILL
PICK-UP LOOP
NIOBIUM FLUX TUBE
THERMAL CONTACT MATERIAL

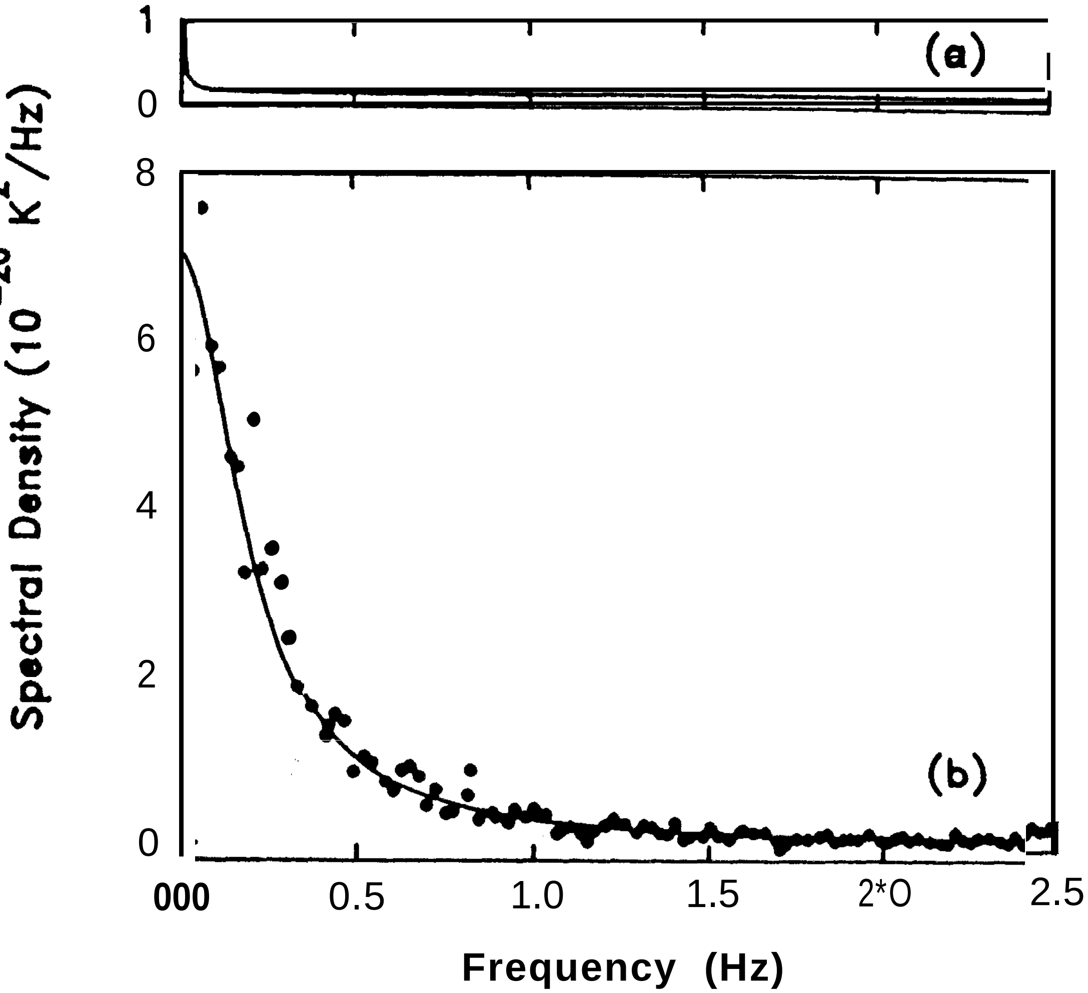

Spectral Density (10^-20 K^2/Hz)
Frequency (Hz)
(a)
(b)
1
0
8
6
4
2
0
000
0.5
1.0
1.5
2*O
2.5

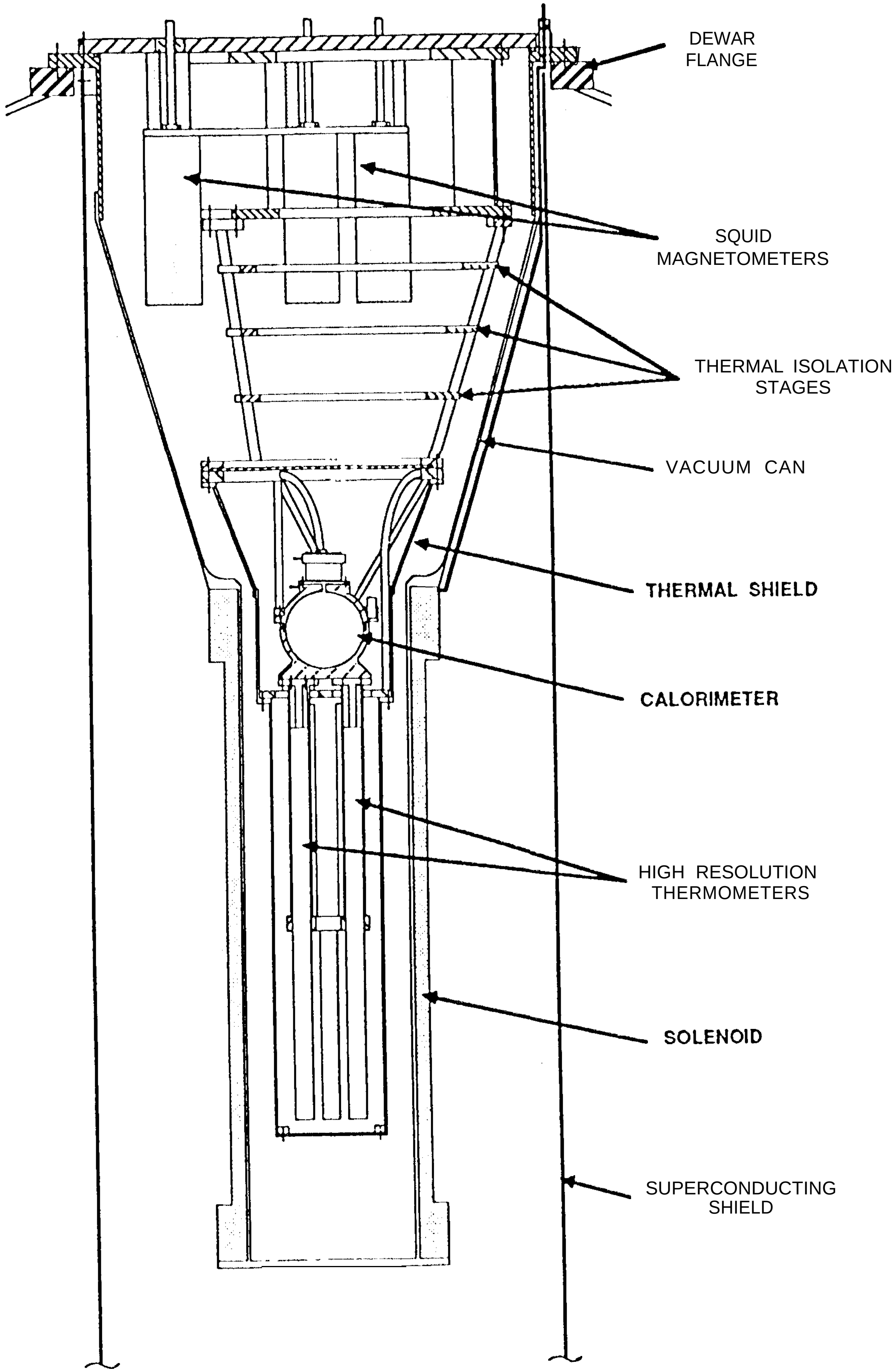
DEWAR FLANGE
SQUID MAGNETOMETERS
THERMAL ISOLATION STAGES
VACUUM CAN
THERMAL SHIELD
CALORIMETER
HIGH RESOLUTION THERMOMETERS
SOLENOID
SUPERCONDUCTING SHIELD

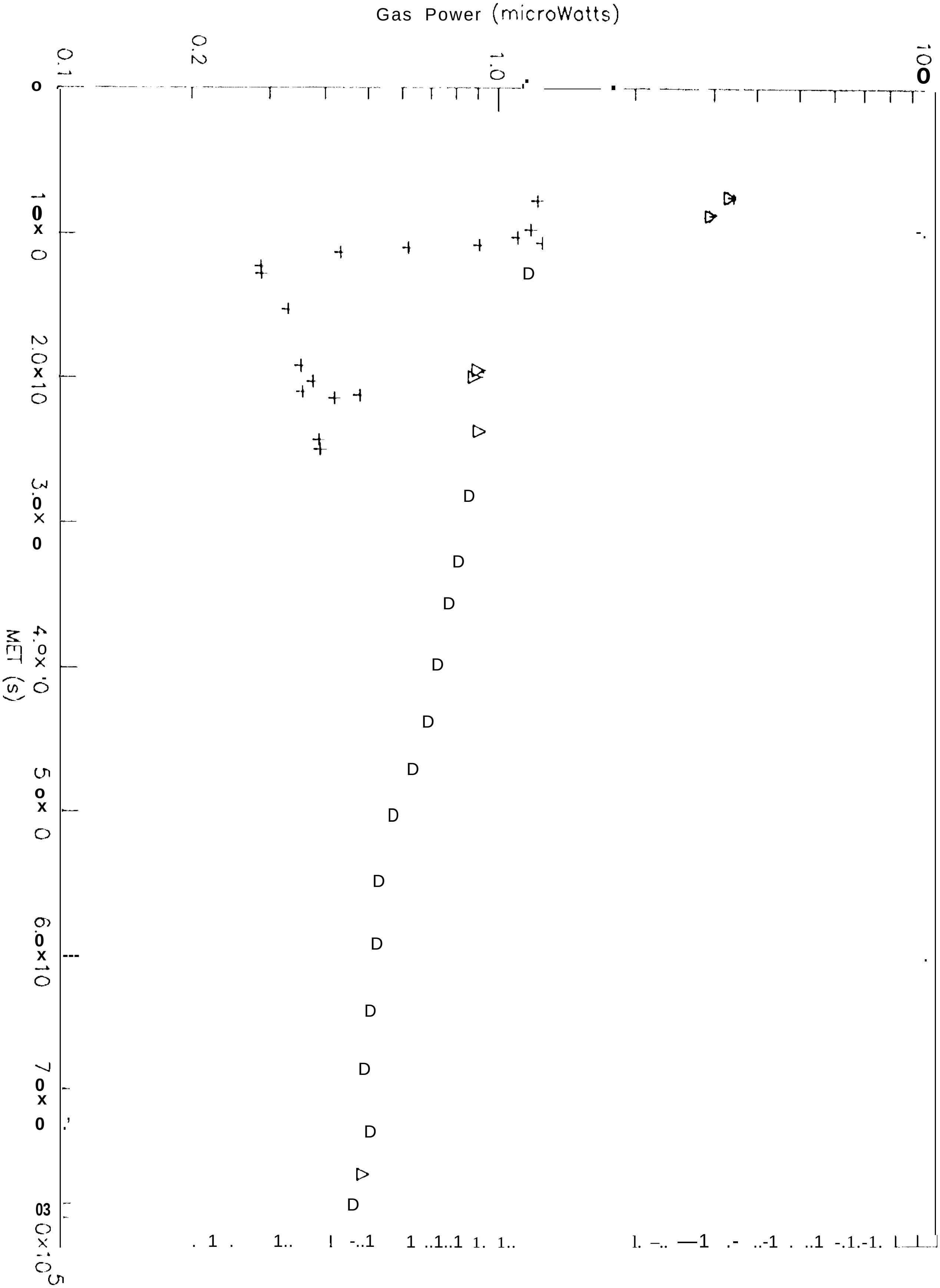

Gas Power (microWatts)
0.1
0.2
1.0
MET (s)
2.0x10

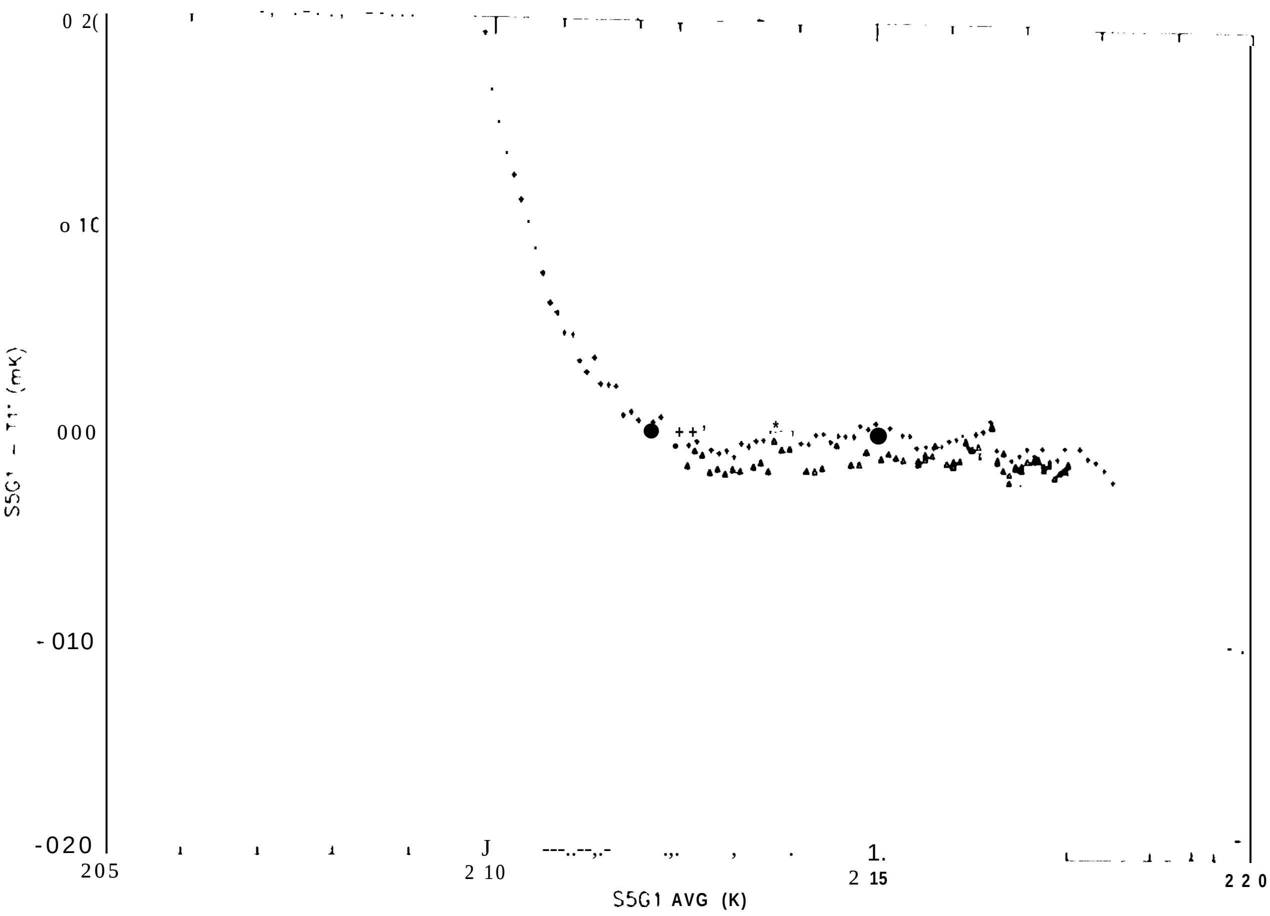

0 2(
o 1C
000
- 010
-020
205
2 10
2 15
2 2 0
S5G' – T1' (mK)
S5G1 AVG (K)

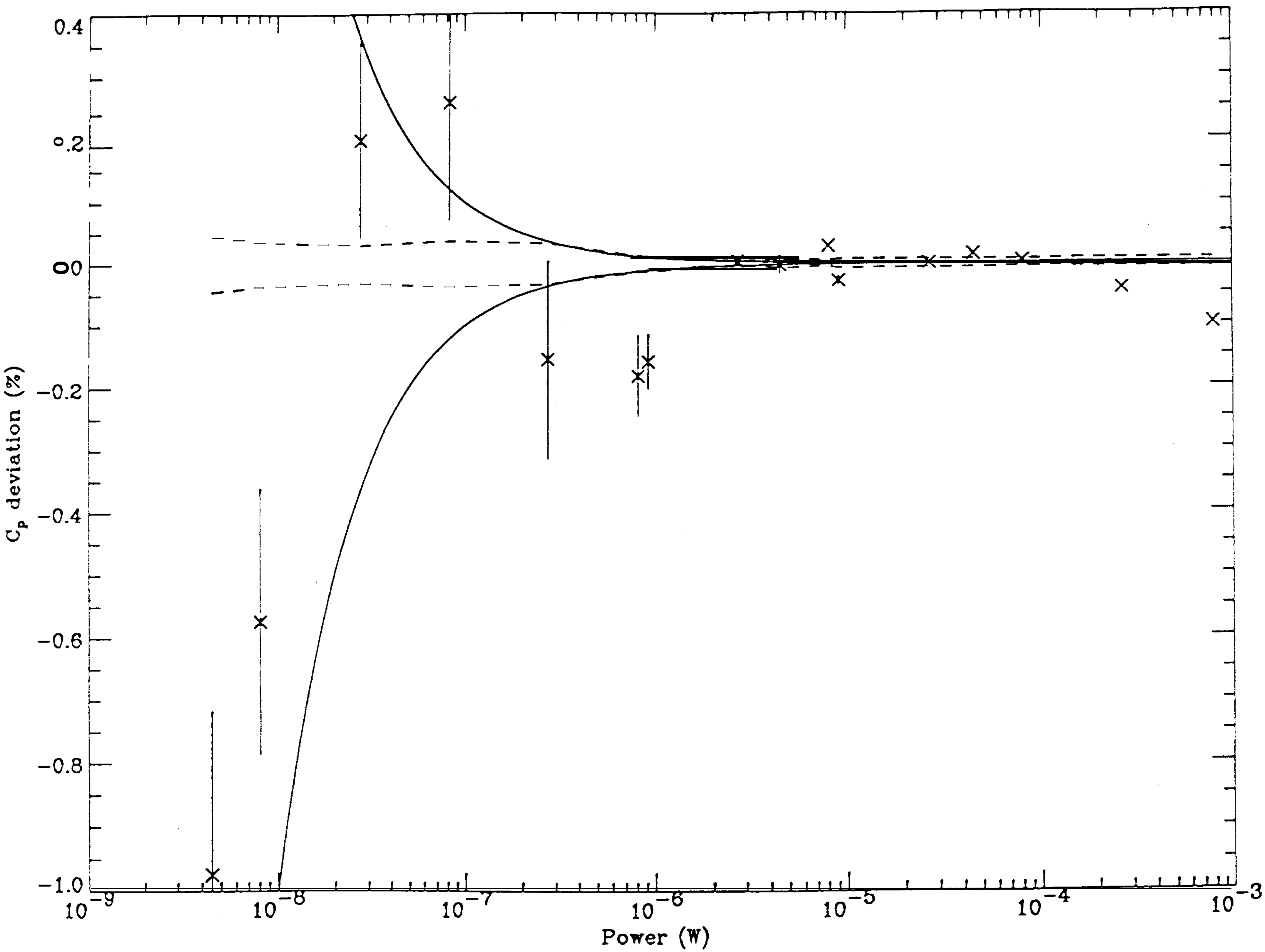

0.4
0.2
0
−0.2
−0.4
−0.6
−0.8
−1.0
$C_p$ deviation (%)
$10^{-9}$
$10^{-8}$
$10^{-7}$
$10^{-6}$
$10^{-5}$
$10^{-4}$
$10^{-3}$
Power (W)

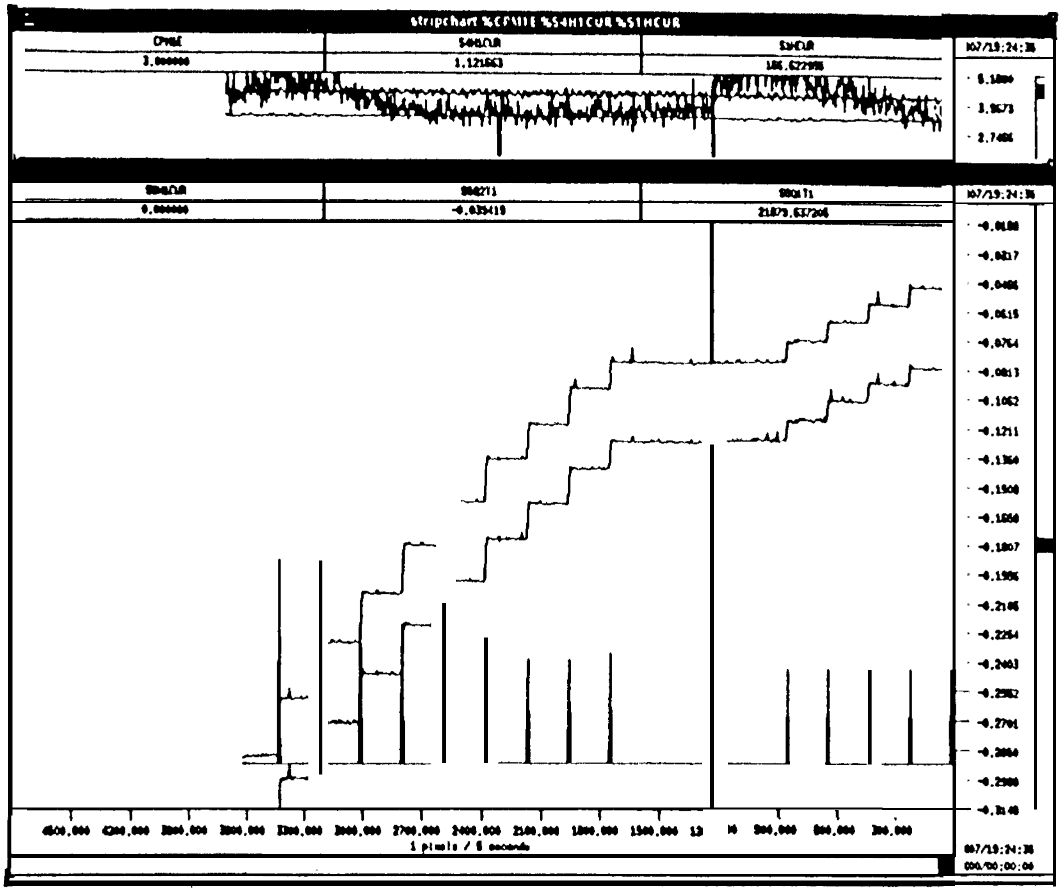

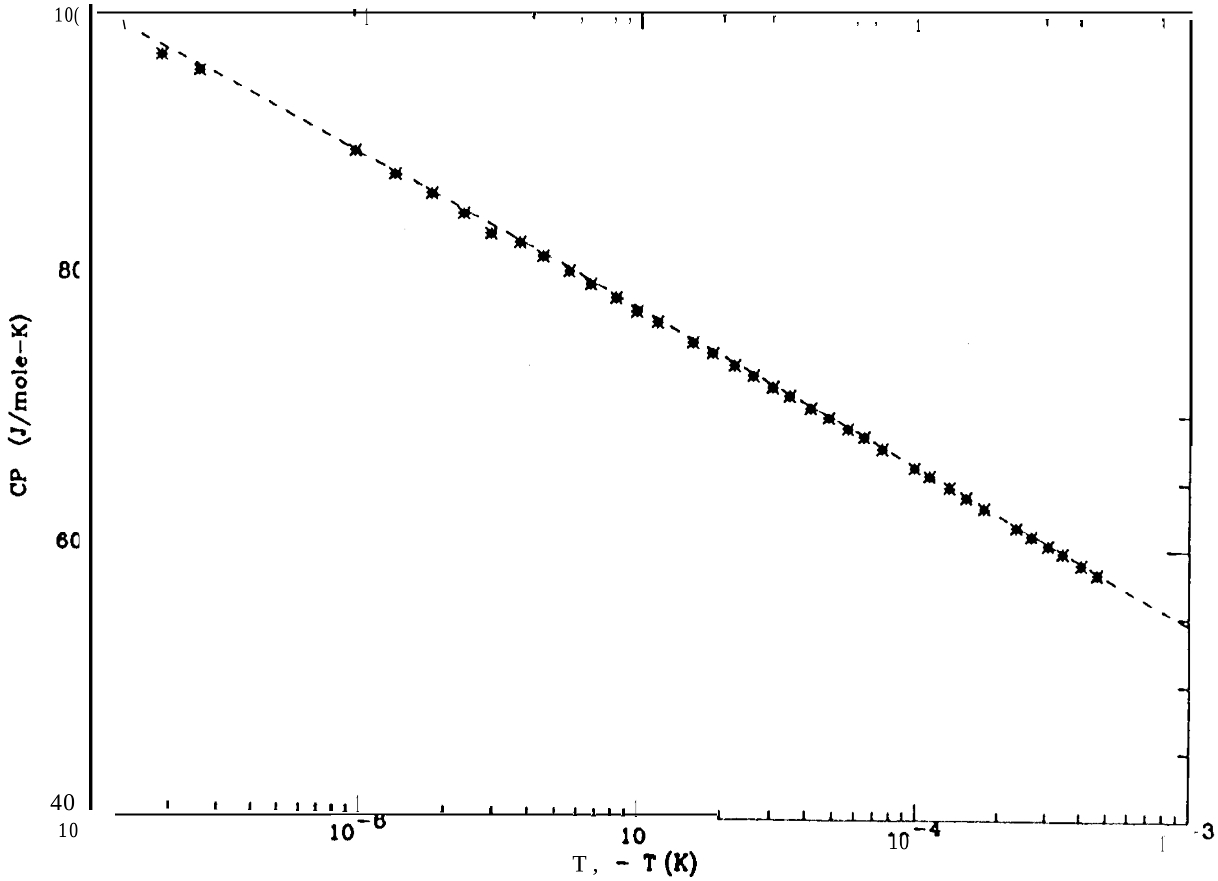

CP (J/mole-K)
10(
8(
6(
40
10
$10^{-6}$
10
$10^{-4}$
-3
T, - T (K)

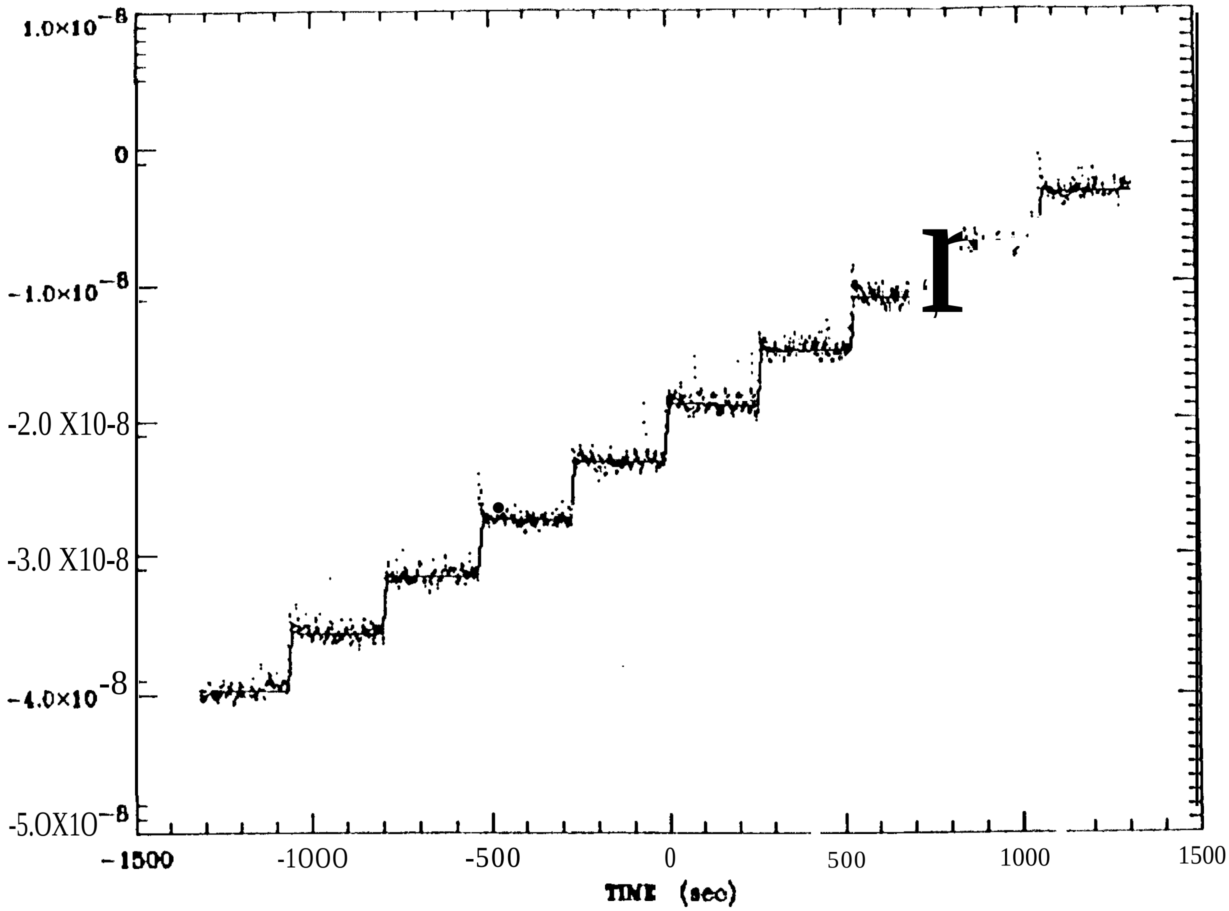
1.0×10⁻⁸
0
-1.0×10⁻⁸
-2.0 X10-8
-3.0 X10-8
-4.0×10⁻⁸
-5.0X10⁻⁸
-1500
-1000
-500
0
500
1000
1500
TIME (sec)

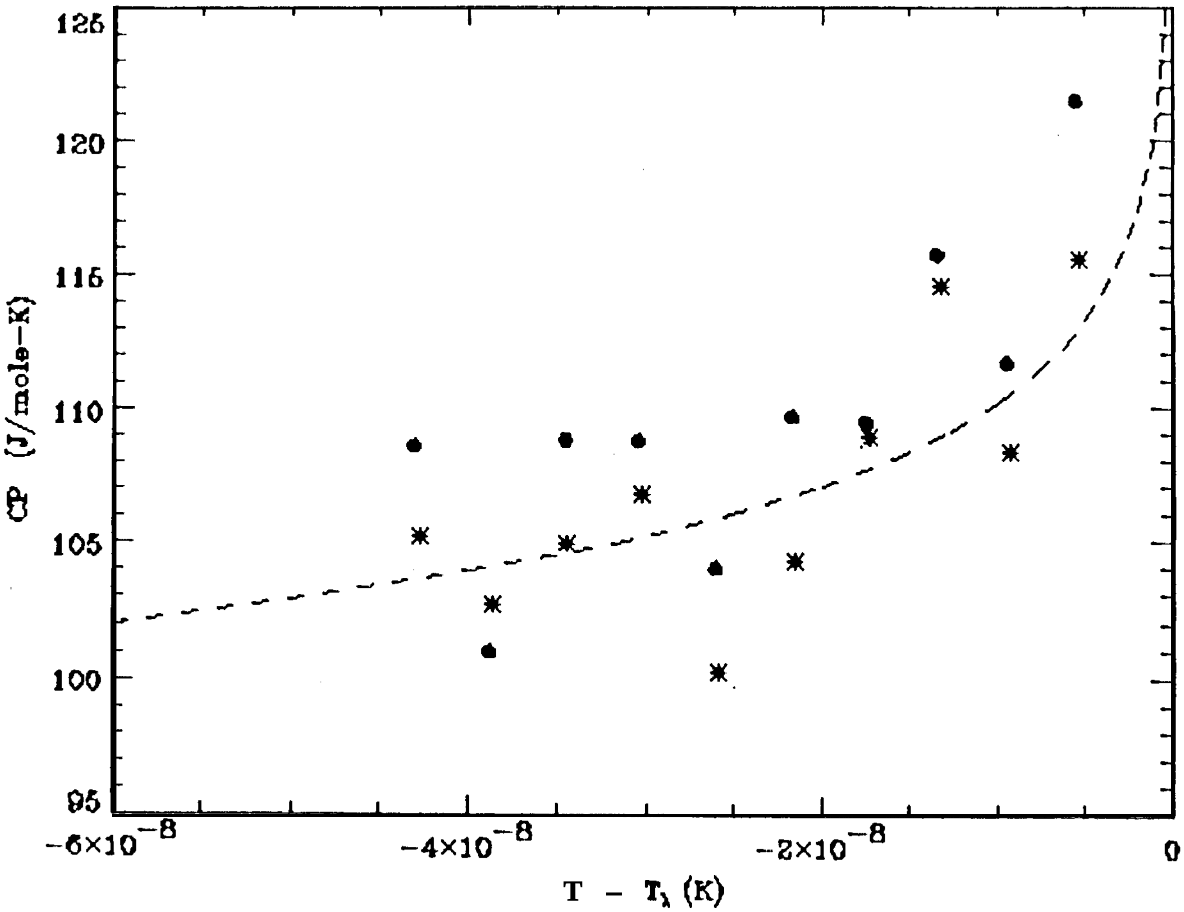

125
120
115
110
105
100
95
CP (J/mole-K)
-6×10^-8
-4×10^-8
-2×10^-8
0
T - Tλ (K)

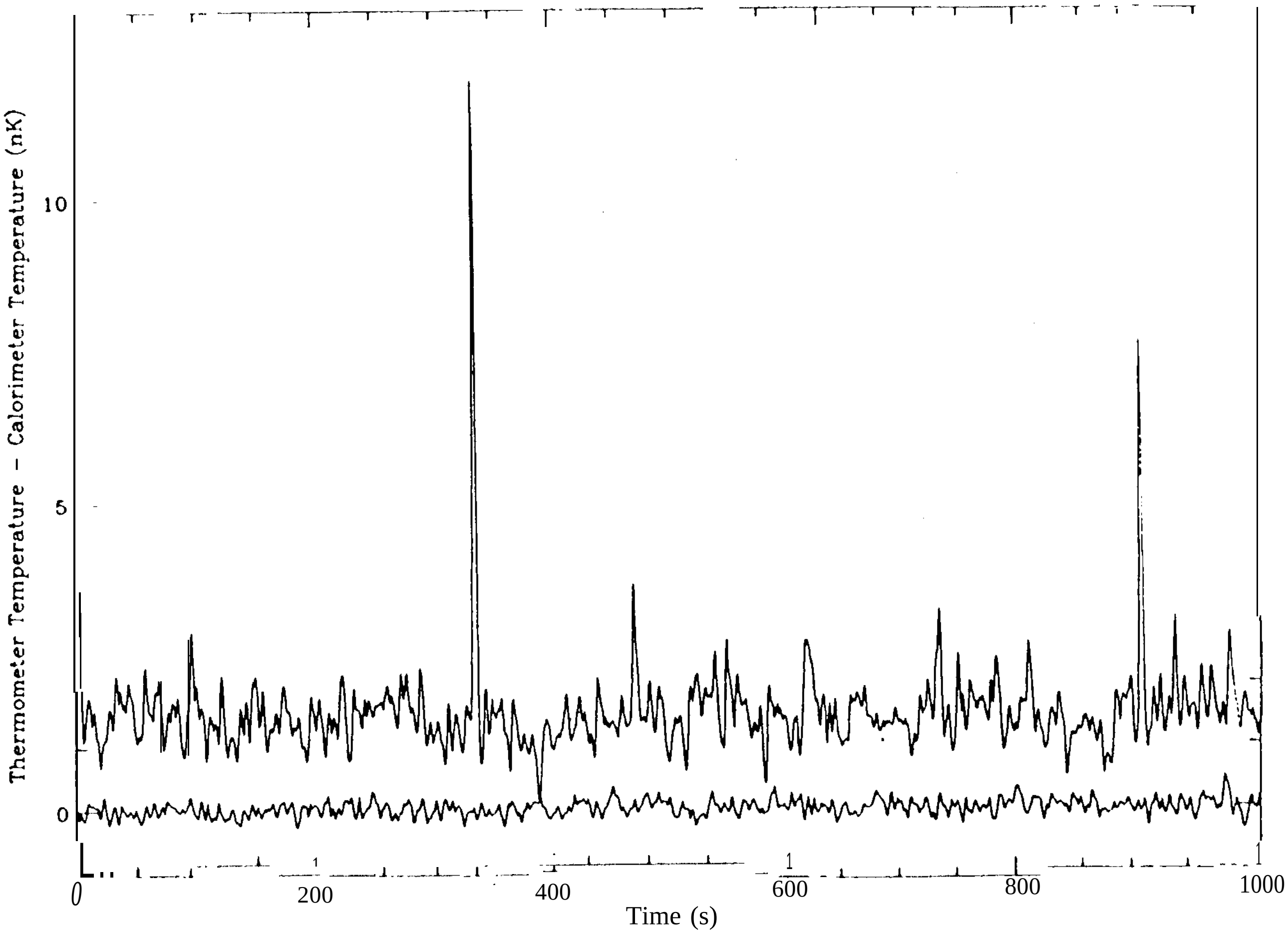

Thermometer Temperature - Calorimeter Temperature (nK)
10
5
0
0
200
400
600
800
1000
Time (s)

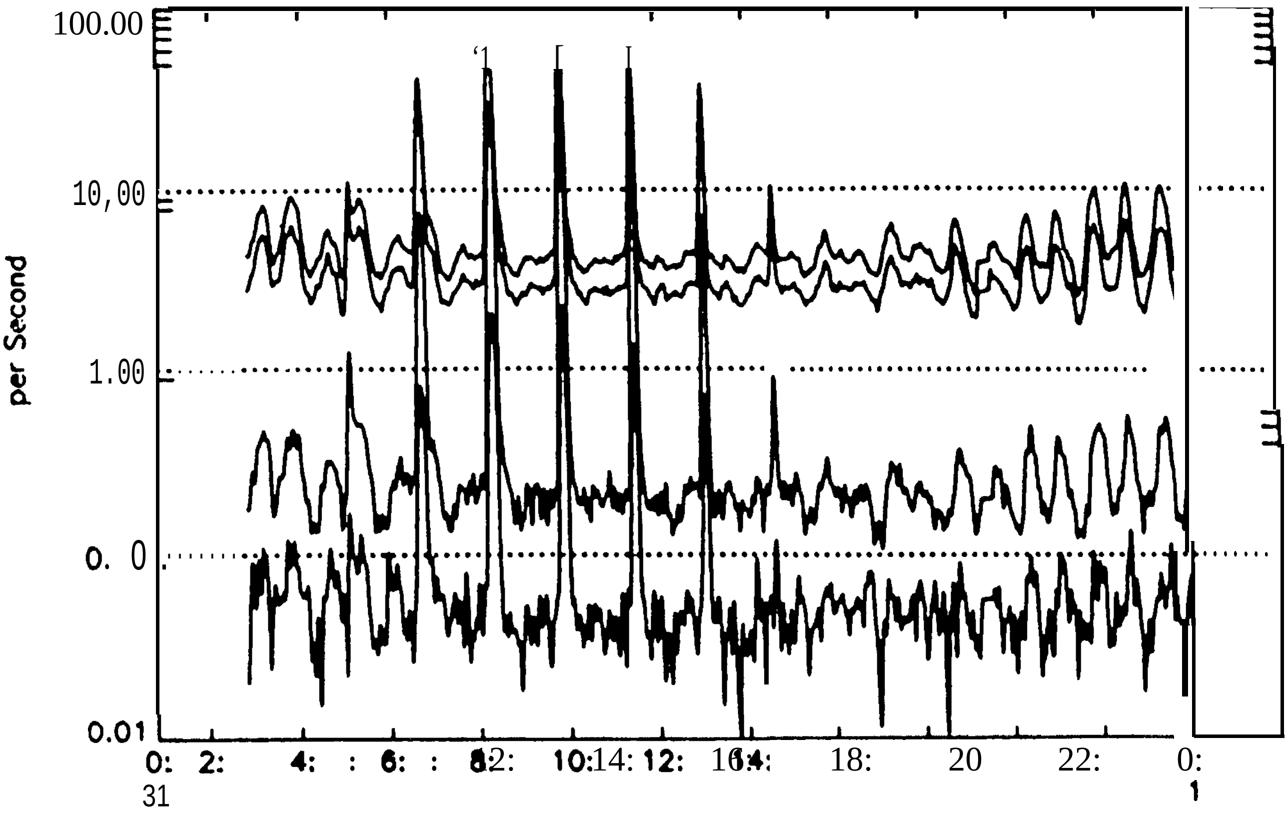

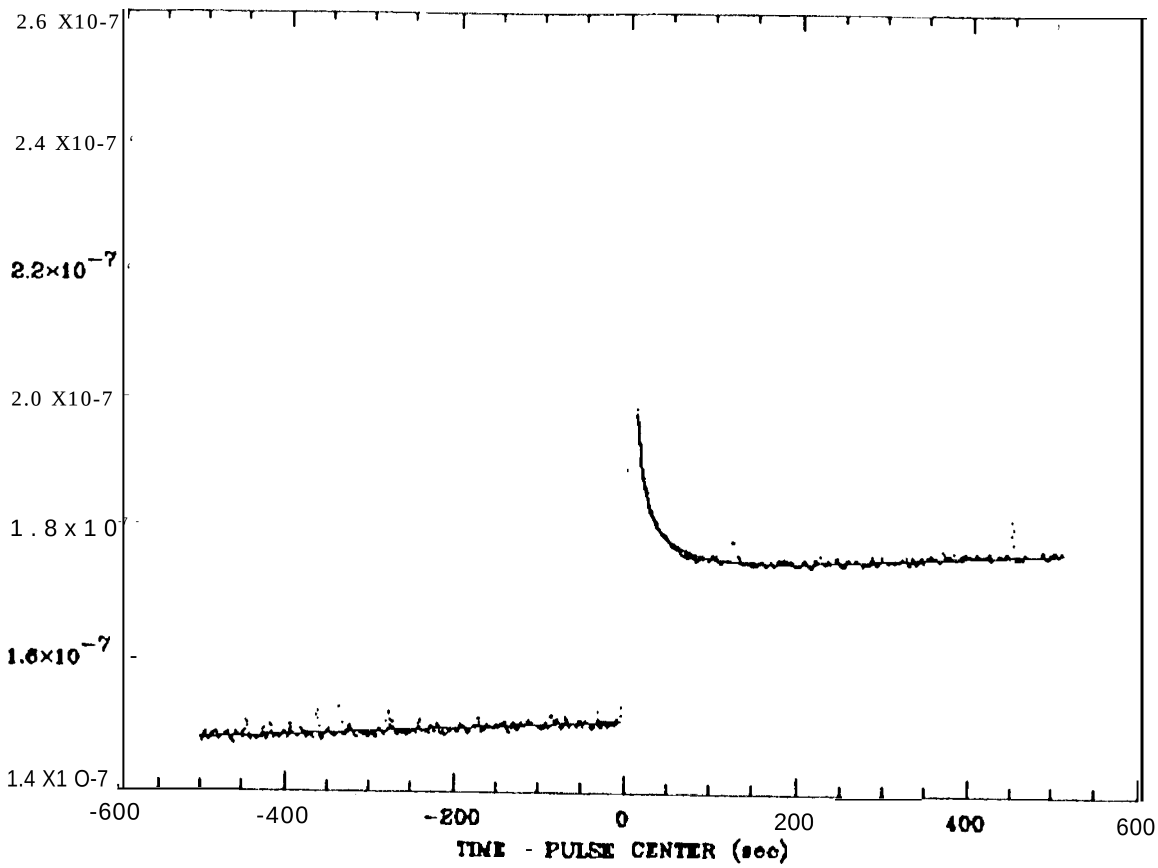

2.6 X10-7
2.4 X10-7
2.2×10$^{-7}$
2.0 X10-7
1.8 x 10$^{-7}$
1.6×10$^{-7}$
1.4 X1 O-7
-600
-400
-200
0
200
400
600
TIME - PULSE CENTER (sec)